

Ultrafast optical generation of carriers in a dc electric field: Transient localization and photocurrent

A. V. Kuznetsov and C. J. Stanton

Department of Physics, University of Florida, 215 Williamson Hall, Gainesville, Florida 32611

(Received 17 June 1993)

Recent experimental observations of terahertz radiation produced by the ultrafast optical excitation of surface depletion layers of GaAs and InP have generated a lot of interest but its physical origins are still not fully understood. The source of the radiation is believed to be either the time-dependent transport current produced by the optically generated carriers in the depletion field, or the displacement current due to creation of polarized electron-hole pairs. We show that, in general, both mechanisms must be included. The ultrafast optical generation in a dc field is shown to result in the creation of carriers in transiently localized states that evolve into delocalized states, causing transport current in the process. By calculating the dipole moments of these localized states, we are able to determine the time-dependent polarization and photocurrent including both transport and displacement contributions. We find that the displacement contribution comes mainly from the virtual carriers while the real carriers are responsible for the transport current. The competition between transport and displacement current leads to a non-trivial dependence of the overall signal on the dc field strength, the excitation duration, and the detuning. In particular, we predict a sign reversal of the signal at sufficiently high detunings in agreement with recent experimental findings.

I. INTRODUCTION

Recently, several experimental groups have demonstrated that the ultrafast optical excitation of bulk semiconductors and semiconductor microstructures subjected to a dc electric field produces submillimeter electromagnetic radiation.¹⁻⁵ There are two general mechanisms for such electromagnetic transients. Originally,¹ this radiation was assumed to result from the acceleration of photoexcited carriers in the electric field in the surface depletion region. The rapid changes in the number of carriers, due to the ultrashort excitation pulse, should lead to a transport photocurrent that changes rapidly in time and emits electromagnetic radiation. However, this explanation is incomplete since the radiation is also present in quantum-confined structures^{2,4} where the transport current is suppressed. In such structures, the optical excitation causes transitions between electronic states that are polarized by the dc field, and the creation of electron-hole pairs in states with a nonzero dipole moment produces a displacement current proportional to the transition rate. The changing displacement current produces the observed radiation.

While there is no reason why the "polarized-pair" argument should not apply to the bulk case as well,^{4,6} it faces difficulties when there are no confining barriers, as in quantum wells, to restrict the movement of carriers along the field. In bulk, since the stationary electron and hole states are delocalized over the entire sample, the dipole moment they acquire in a dc field is proportional to the size of the sample. This seems unphysical, but if we place an electron-hole pair in a biased sample and wait long enough, the electron and the hole will be pushed against the opposite walls of the sample creating a dipole moment proportional to its size.

This size dependence is not an artifact and should be present at least in the steady-state limit of Refs. 4 and 6. However, with increasing sample size it will take carriers increasingly longer to separate (a simple estimate shows that it would take a few picoseconds for an $e-h$ pair in GaAs to cross a $1\text{-}\mu\text{m}$ sample in a 1-kV/cm dc field). The time needed to reach the steady-state limit is therefore at least an order of magnitude greater than the excitation duration. In addition, stationary states themselves carry no current, so that in Refs. 4 and 6 there is never any transport current in bulk samples which is clearly incorrect. For the above reasons steady-state theories are not applicable to *femtosecond* excitation conditions. This applies also to the transport current calculations^{7,8} that use the semiclassical Boltzmann equation because the latter does not include quantum-mechanical coherence between electronic states that is essential at times shorter than the relaxation time. Therefore, one has to use a more elaborate approach to the description of carrier transport during and immediately after the femtosecond optical excitation.

In this paper we present a theory that can treat *both* transport and displacement current within the *same* formalism. We demonstrate that to get a consistent picture of ultrafast transport phenomena, it is necessary to consider the excitation process in real time. The key element of our approach is a full time-dependent quantum-mechanical treatment of optical transitions. For short pulses the transition energy is not well defined, and one can no longer use the conventional picture of energy-conserving interband transitions. In the presence of the dc field, the eigenstates are no longer characterized by a single \mathbf{k} vector. As a result, an electron in the valence band can be optically excited into more than one state in the conduction band, unlike the zero-field case. The final

state after optical excitation is then a localized wave packet formed by a coherent superposition of delocalized states with different energies. The dipole moment of these wave packets can be calculated and is independent of the sample size. Its time derivative gives both the transport and displacement currents. To simplify our analysis of wave-packet dynamics we neglect the Coulomb interaction (excitonic effects) and other relaxation processes.

The paper is organized as follows. Section II introduces the Airy representation for electron states in a semiconductor and presents a density-matrix approach to the quantum-mechanical description of this system. In Sec. III we discuss how observables such as the charge density and the dipole moment can be calculated through the intraband density matrix, and study several relevant limiting cases. Section IV contains numerical results for the dielectric polarization and its derivatives—the photocurrent and radiated signal—along with a brief discussion of their dependence on the dc field and other parameters of the problem. Our conclusions are given in Sec. V.

II. DENSITY-MATRIX FORMALISM IN THE AIRY REPRESENTATION

In this section we introduce our model and derive the equations that govern carrier dynamics during and after ultrafast photoexcitation in the absence of relaxation processes. We consider an ideal direct-gap semiconductor with two parabolic bands c (conduction) and v (valence) in a uniform stationary electric field $F = eE$ acting along the x axis. Although in realistic depletion layers the field is nonuniform and varies on the length scale of a few micrometers, we will see below that the length scales relevant for coherent carrier dynamics are typically much shorter so that the field can be considered uniform.

A. Eigenstates in a dc electric field

Our first step will be to determine the electronic eigenstates. In the plane perpendicular to the dc field the eigenstates are still plane waves, and since we are not considering any scattering processes or the Coulomb effects, these states are completely uncoupled. However, in the direction along the dc field the eigenstates have to be modified. In a finite-size sample this could be done by perturbatively correcting the plane-wave states, but we find it more convenient to use exact eigenstates for an unbounded sample which can be expressed in terms of Airy functions.⁹ Because of the need to satisfy the boundary conditions on the walls of the sample, our treatment will work only when the sample size is much greater than the characteristic period of the eigenfunctions, which imposes a lower limit on the dc field in our theory. We will discuss the corresponding quantitative criteria more fully below.

We disregard the effect of the dc field on the periodic part of the crystal wave functions and consider only the envelope, ψ , because the field-induced changes in the periodic part are small as long as the dc fields are small compared to the atomic fields. The eigenstates in the x

direction are the solutions to the Schrödinger equation:

$$\frac{\partial^2 \psi}{\partial x^2} + \frac{2m_\alpha}{\hbar^2} (\nu + Fx) \psi = 0. \quad (1)$$

Here, $\alpha = (c, v)$ is the band index and ν is the energy eigenvalue. The Fourier transform of this equation,

$$-k^2 \psi(k) + \frac{2m_\alpha}{\hbar^2} \nu \psi(k) = i \frac{2m_\alpha F}{\hbar^2} \frac{\partial \psi}{\partial k}, \quad (2)$$

can be integrated directly, which yields the eigenfunction in k space:

$$\psi_{\nu,}(k) = \frac{1}{\sqrt{2\pi F}} \exp \left\{ -i\nu \frac{k}{F} + i \frac{\hbar^2 k^3}{6m_\alpha F} \right\}. \quad (3)$$

We can restore the real-space eigenfunction by performing the inverse Fourier transform of (3):

$$\begin{aligned} \psi_{\nu,}(x) &= \int dk \psi_{\nu,}(k) e^{-ikx} \\ &= \frac{1}{\sqrt{2\pi F}} \int dk \exp \left\{ -i\nu \frac{k}{F} - ikx + i \frac{\hbar^2 k^3}{6m_\alpha F} \right\} \\ &= \frac{2}{\sqrt{2\pi F}} \int_0^\infty \cos \left\{ k \left[x + \frac{\nu}{F} \right] - \frac{\hbar^2 k^3}{6m_\alpha F} \right\} dk. \end{aligned} \quad (4)$$

Note that (a) the eigenfunctions are now superpositions of different k states and therefore do not correspond to a distinct value of the wave vector; (b) they have an essential singularity as a function of the dc field and therefore the field cannot be treated as a perturbation; (c) we do not write explicitly the wave functions for the y - z plane—they are plane waves $\exp(ik_y y + ik_z z)$ characterized by quantum numbers $k_\perp = (k_y, k_z)$. For a given k_\perp , the effective band gap will be $E_g^1 = E_g + (\hbar^2/2m_r)k_\perp^2$, where $m_r = m_c m_v / (m_c + m_v)$ is the reduced mass. We will concentrate on the behavior of quantities of interest in the field direction and will therefore consider states with the same fixed value of the perpendicular momentum.

At this point it is advantageous to introduce dimensionless variables. We define a field-dependent unit of length:

$$l_0 \equiv \left(\frac{\hbar^2}{2m_r F} \right)^{1/3}, \quad (5)$$

as well as units of energy and time:

$$\varepsilon_0 \equiv F l_0 = \left(\frac{\hbar^2 F^2}{2m_r} \right)^{1/3}, \quad \tau_0 \equiv \frac{\hbar}{\varepsilon_0} = \left(\frac{2m_r \hbar}{F^2} \right)^{1/3}. \quad (6)$$

For further reference, we rewrite (5) and (6) using the parameters of GaAs ($m_r = 0.061m_0$):

$$\begin{aligned} l_0 &= 37.3 \text{ nm} \times F^{-1/3} \text{ (kV/cm)}, \\ \varepsilon_0 &= 3.73 \text{ meV} \times F^{1/3}, \\ \tau_0 &= 167 \text{ fs} \times F^{-2/3}. \end{aligned} \quad (7)$$

From now on we will measure all distances, energies, and times in units (5) and (6). In dimensionless units the wave functions (4) become

$$\psi_v^c(x) = \left[\frac{2}{F} \right]^{1/2} \beta_c \frac{1}{l_0} \text{Ai}[-\beta_c(x + \nu)] \quad (8)$$

for the conduction-band electrons and

$$\psi_v^v(x) = \left[\frac{2}{F} \right]^{1/2} \beta_v \frac{1}{l_0} \text{Ai}[\beta_v(x - \nu)] \quad (9)$$

for the valence-band electrons (which have negative mass, hence the sign difference). Note that the conduction- and valence-band states with equal ν have energy difference E_g^\perp . Here, $\beta_\alpha = (m_\alpha/m_r)^{1/3}$ and

$$\text{Ai}(x) = \frac{1}{\sqrt{\pi}} \int_0^\infty du \cos \left[ux + \frac{u^3}{3} \right] \quad (10)$$

is the Airy function.⁹ Note that for all energies ν , the eigenfunctions (8) and (9) are in fact the same function shifted along the x axis by an appropriate amount. Thus, the energy dependence of the wave functions corresponds to a shift in space.

It is easily verified that the eigenfunctions are orthogonal within each band:

$$\int dx \psi_v^{c*}(x) \psi_\lambda^c(x) \equiv \langle \psi_v^c | \psi_\lambda^c \rangle = 2\pi \delta(\nu - \lambda) = \langle \psi_v^v | \psi_\lambda^v \rangle. \quad (11)$$

We will also need the overlap integral of eigenfunctions from different bands:

$$\chi_{\lambda\nu}^{vc} \equiv \langle \psi_\lambda^v | \psi_\nu^c \rangle = \langle \psi_\nu^c | \psi_\lambda^v \rangle = \frac{1}{\varepsilon_0 \sqrt{\pi}} \text{Ai}(\lambda - \nu). \quad (12)$$

Strictly speaking, the above-defined Airy function eigenstates are applicable only to an unbounded sample, because for a finite-size sample they do not strictly satisfy the boundary conditions. In general the solution of the Schrödinger equation (1) should be a superposition of $\text{Ai}(x)$ and $\text{Bi}(x)$ (the other Airy function that diverges exponentially at positive argument).⁹ However, for the case where l_0 is much smaller than the sample size, the functions $\text{Ai}(x)$ are an excellent approximation to the exact eigenstates because they are exponentially small at positive arguments and can be taken to be zero at one of the walls, while at negative arguments they are oscillating rapidly and can easily satisfy the other boundary condition as well. Since the field-dependent length l_0 will approach the sample size for *decreasing dc fields*, our analysis breaks down in the limit of *weak dc fields*, so that we cannot formally recover linear-response results or other weak-field properties (the formal reason is the above-mentioned singularity of the wave functions). However, this is more of a technical difficulty rather than a real limitation, because, e.g., for a 1- μm sample the condition $L \gg l_0$ is satisfied for dc fields greater than 0.1 V/cm. Since typical depletion fields are in the kV/cm range, our analysis should work well for relevant experimental situations.

B. Density matrix in a dc electric field

Now we can define the density matrix using the states (8) and (9) as a basis. Let $a_{\alpha\nu}^\dagger(t)$ and $a_{\alpha\nu}(t)$ denote the

Heisenberg operators that create and annihilate electrons in an eigenstate ν of the band α . The density matrix (DM) is defined as

$$\begin{aligned} N_{\nu\lambda}^{\alpha\beta}(t) &\equiv \langle a_{\alpha\nu}^\dagger(t) a_{\beta\lambda}(t) \rangle \\ &= \left[\begin{array}{cc} \langle a_{c\nu}^\dagger a_{c\lambda} \rangle & \langle a_{c\nu}^\dagger a_{v\lambda} \rangle \\ \langle a_{v\nu}^\dagger a_{c\lambda} \rangle & \langle a_{v\nu}^\dagger a_{v\lambda} \rangle \end{array} \right]_{\alpha\beta} \\ &= \left[\begin{array}{cc} n_{\nu\lambda}^c & p_{\nu\lambda} \\ p_{\lambda\nu}^* & n_{\nu\lambda}^v \end{array} \right]_{\alpha\beta}, \end{aligned} \quad (13)$$

where $\langle \rangle$ denotes the statistical average over the current nonequilibrium state of the system.

Note that $p_{\nu\lambda}$ is *not* the density of holes but the inter-band component of the DM which describes the coherence between states λ and ν from different bands and is related to the optical polarization.^{10,11} The intraband components $n_{\lambda\nu}^\alpha$ describe correlations between different eigenstates λ, ν within the same band and have no classical equivalent except for $n^\alpha(\lambda = \nu)$, which is just the number of particles in the state λ (note that $n_{\lambda\lambda}^v$ is the number of valence band electrons rather than holes, cf. Eq. (33) below).

C. Equation of motion for the density matrix

The density matrix obeys the general equation of motion

$$i \frac{\partial \hat{N}}{\partial t} = \langle [\hat{H}, \hat{N}] \rangle, \quad (14)$$

where the square brackets denote matrix commutator. The Hamiltonian in (14) has the following form for the system without interactions:

$$\hat{H}_0 = \sum_{\alpha\lambda} \varepsilon_{\alpha\lambda} a_{\alpha\lambda}^\dagger a_{\alpha\lambda}, \quad (15)$$

where

$$\varepsilon_{c\lambda} = E_g + \lambda + \frac{\hbar^2}{2m_c} k_\perp^2, \quad \varepsilon_{v\lambda} = \lambda - \frac{\hbar^2}{2m_v} k_\perp^2 \quad (16)$$

are the energies of the corresponding eigenstates. Taking the commutator in (14), we get the following equation for the free-electron DM:

$$\frac{\partial N_{\nu\lambda}^{\alpha\beta}}{\partial t} = i(\varepsilon_{\alpha\nu} - \varepsilon_{\beta\lambda}) N_{\nu\lambda}^{\alpha\beta}. \quad (17)$$

Introducing the energy matrix

$$\hat{\varepsilon} = \varepsilon_{\nu\lambda}^{\alpha\beta} \equiv \varepsilon_{\alpha\nu} \delta_{\nu\lambda}^{\alpha\beta}, \quad (18)$$

we can rewrite (17) in matrix form:

$$\frac{\partial N_{\nu\lambda}^{\alpha\beta}}{\partial t} = i \sum_{\gamma\rho} \varepsilon_{\nu\rho}^{\alpha\gamma} N_{\rho\lambda}^{\gamma\beta} - N_{\nu\rho}^{\alpha\gamma} \varepsilon_{\rho\lambda}^{\gamma\beta} \equiv -i[\hat{N}, \hat{\varepsilon}], \quad (19)$$

which proves to be more convenient for incorporating the interaction with the optical field.¹⁰

To take account of the optical excitation, we write the Hamiltonian that couples the electrons to the optical field $E(t)$ within the dipole approximation:

$$\hat{H}_{\text{opt}} = -E(t)\hat{d} = -E(t) \sum_{\alpha\beta\nu\lambda} d_{\nu\lambda}^{\alpha\beta} a_{\alpha\nu}^{\dagger} a_{\beta\lambda}. \quad (20)$$

Here, d is the dipole moment operator. Neglecting intraband optical transitions, we can express the dipole matrix element as

$$d_{\nu\lambda}^{\alpha\beta} = \begin{bmatrix} 0 & \mu_{cv}\chi_{\nu\lambda}^{cv} \\ \mu_{vc}\chi_{\nu\lambda}^{vc} & 0 \end{bmatrix}_{\alpha\beta} \quad (21)$$

with μ being the interband matrix element, and χ is the overlap factor (12). It is important to note that the dc field breaks the wave-vector selection rule for interband transitions. The overlap integral (12) does not have a δ -function structure (of course in the y - z plane the wave-vector selection rule still works). This means that *interband light couples a given valence-band state to the whole conduction band*, making the situation very different from the two-level system picture¹¹ of the zero-field case.

Because the interaction Hamiltonian (20) contains only pairs of second-quantization operators, the commutator in the equation of motion (14) can be taken exactly. To account for the effect of the optical field on the DM evolution, we only need to renormalize the energy matrix in (19) (see Ref. 10 for details):

$$\hat{\epsilon}_R = \hat{\epsilon} + \hat{M} = \epsilon_{\nu\lambda}^{\alpha\beta} + M_{\nu\lambda}^{\alpha\beta}(t), \quad (22)$$

where we have denoted

$$M_{\nu\lambda}^{\alpha\beta}(t) \equiv d_{\nu\lambda}^{\alpha\beta} E(t). \quad (23)$$

The equation of motion basically keeps the form (19) in the presence of an optical field:

$$\begin{aligned} \frac{\partial N_{\nu\lambda}^{\alpha\beta}}{\partial t} &= -i[\hat{N}, \hat{\epsilon}_R] \\ &= i(\epsilon_{\alpha\nu} - \epsilon_{\beta\lambda})N_{\nu\lambda}^{\alpha\beta} - i \sum_{\gamma\rho} \{N_{\nu\rho}^{\alpha\gamma} M_{\rho\lambda}^{\gamma\beta} - M_{\nu\rho}^{\alpha\gamma} N_{\rho\lambda}^{\gamma\beta}\}. \end{aligned} \quad (24)$$

This is a generalization of the optical Bloch equations^{10,11} to include a dc electric field. Using the expression for M , Eq. (23), we can extract from Eq. (24) the equation for the interband DM components by setting $\alpha=c$ and $\beta=v$:

$$\begin{aligned} \frac{\partial p_{\nu\lambda}}{\partial t} &= i(\epsilon_{cv} - \epsilon_{v\lambda})p_{\nu\lambda} \\ &+ i\mu_{cv} E(t) \int d\rho \{n_{\rho\lambda}^v \chi_{\nu\rho}^{cv} - n_{\nu\rho}^c \chi_{\rho\lambda}^{cv}\}. \end{aligned} \quad (25)$$

The first term in Eq. (25) represents free oscillations of

the polarization. The quantity in the curly brackets in the driving term is a generalized saturation term.

If we consider only the low-excitation case here, we can simplify it by setting $n_{\nu\lambda}^c = 0$ and $n_{\nu\lambda}^v = \delta(\nu - \lambda)$, since in a nonexcited (and undoped) semiconductor we have an empty conduction band and a full valence band without intraband correlations. With these assumptions, Eq. (25) becomes

$$\frac{\partial p_{\nu\lambda}}{\partial t} = i(\epsilon_{cv} - \epsilon_{v\lambda})p_{\nu\lambda} + i\mu_{cv} E(t) \chi_{\nu\lambda}^{cv}. \quad (26)$$

An equation for the intraband DM can also be retrieved from (24) by setting $\alpha, \beta = c$:

$$\begin{aligned} \frac{\partial n_{\nu\lambda}^c}{\partial t} &= i(\nu - \lambda)n_{\nu\lambda}^c - i\mu_{cv} \int d\rho \{p_{\nu\rho} \chi_{\rho\lambda}^{vc} E^* \\ &- \chi_{\nu\rho}^{cv} p_{\rho\lambda}^* E\} \end{aligned} \quad (27)$$

(we do not write out the equation for the holes since it has similar structure). As is seen from (27), the carriers are created due to interaction of the field with the polarization (25), and because of the above-mentioned absence of strict selection rules for the polarization the electronic states also become correlated within each band in a finite range of $\lambda - \nu$.

Equations (26) and (27) could have been obtained more readily through time-dependent perturbation theory in the optical field. However, the original equation (24) of the density-matrix formalism is more general and can be applied to the high-excitation case as well.

D. Solution for the density matrix in the low-excitation limit

In the low-excitation limit, we can actually solve (27) analytically. Representing the optical field as

$$E(t) = E_0 f(t) e^{i\omega t}, \quad (28)$$

we can directly integrate (26) and get the following result:

$$p_{\nu\lambda}(t) = i\mu_{cv} \chi_{\nu\lambda}^{cv} E_0 F_R(t, \nu - \lambda - \Delta). \quad (29)$$

Here $\Delta = \omega - E_g^\perp \equiv \omega - E_g - \hbar^2 k_\perp^2 / 2m_r$ is the detuning, and F_R is the retarded Fourier transform of the pulse envelope defined as

$$F_R(t, \Omega) = \tau_0 \int_{-\infty}^0 d\tau f(t + \tau) e^{-i\Omega\tau}. \quad (30)$$

Substituting (29) for polarization in (27), we directly integrate the resulting differential equation, which gives, after some algebra, the following expression for the intraband density matrix:

$$n_{\nu\lambda}^c(t) = |\mu_{cv}|^2 E_0^2 \tau_0 \int_{-\infty}^t dt' f(t') e^{i(\lambda - \nu)[t' - t]} \int d\rho \chi_{\lambda\rho}^{cv} \chi_{\rho\nu}^{vc} \{F_R^*(t', [\lambda - \rho] - \Delta) + F_R(t', [\nu - \rho] - \Delta)\}. \quad (31)$$

Equation (31) makes it clear that intraband DM depends only on the *difference* of its energy arguments, $\lambda - \nu$, so that we can set $\lambda = 0$ and consider $n_{\lambda\nu}^c(t)$ the function of the energy difference ν . Substituting (12) for χ 's in (31), we arrive at

$$n^c(t, \nu) = \frac{m_0}{\pi^2 \hbar^2} \frac{|\mu_{cv}|^2 E_0^2}{F^2} \int_{-\infty}^t dt' f(t') e^{i\nu[t' - t]} \times \int d\rho \text{Ai}(-\rho) \text{Ai}(-\nu - \rho) \{F_R^*(t', \rho - \Delta) + F_R(t', \rho + \nu - \Delta)\}. \quad (32)$$

Finally, by similar steps we get the following results for the density matrix of the holes:

$$n_{\nu\lambda}^h \equiv \delta_{\nu\lambda} - n_{\nu\lambda}^v = n_{\nu-\Delta, \lambda-\Delta}^c, \quad (33)$$

which indicates that the hole states $\nu-\Delta, \lambda-\Delta$ are correlated in exactly the same way as states ν, λ in the conduction band. The reasons for this can be seen in Fig. 1. Optical excitation with the photon energy $\hbar\omega = E_g^\perp + \Delta$ couples a given conduction-band state to a state in the valence band that has matching energy eigenvalue; according to the expressions (8) and (9) for the eigenfunctions, the excess energy Δ shifts the valence-band eigenstate by Δ/F along the dc field.

Equation (32) is the main result of this section, and below we will consider it in more detail. Let us first examine more closely the inner integral in (32), assuming Δ to be positive (see Fig. 2). The quantity in curly brackets there generally consists of two identical peaks (30) centered around $\rho = \Delta$ and $\rho = \Delta + \nu$, with the width of the order of the inverse pulse duration, τ_p^{-1} . These peaks are multiplied by the product of two Airy functions, which for large ρ can be replaced by the asymptotic expression⁹

$$\text{Ai}(-\rho) \approx \frac{1}{\sqrt{\pi}} \rho^{-1/4} \sin \left[\frac{2}{3} \rho^{3/2} + \frac{\pi}{4} \right]. \quad (34)$$

The combination of Airy functions entering (32) can therefore be approximately represented as

$$\text{Ai}(-\rho)\text{Ai}(-\rho-\nu) \approx \frac{1}{2\pi\sqrt{\rho}} (\cos[v\sqrt{\rho}] - \sin[\frac{4}{3}\rho^{3/2}]). \quad (35)$$

Around $\rho = \Delta$ this product will have a fast-oscillating component represented by the second term in (35) along with a regular part (the first term) which at $\nu \rightarrow 0$ does not oscillate at all. If the width of the Fourier transforms F_R in (32) is small compared to the period of these fast oscillations (i.e., if $\tau_p \gg 4\pi\sqrt{\Delta}$), we can regard them as δ functions and Eq. (32) reduces to

$$n^c(t, \nu) \approx C \delta(\nu) \text{Ai}^2(-\Delta) \int_{-\infty}^t dt' f^2(t') \quad (36)$$

[where C stands for the prefactor in Eq. (32)].

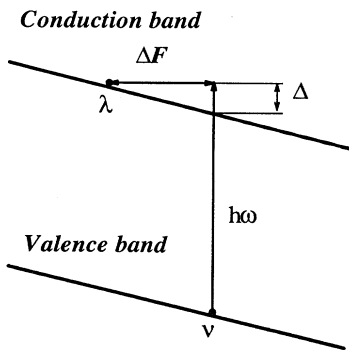


FIG. 1. Optical excitation with the photon energy $\hbar\omega = E_g + \Delta$ couples the state λ in the conduction band to the state ν in the valence band, so that the coordinate space for the holes is shifted by Δ/F along the dc field.

After integration over Δ (i.e., over k_\perp , see Sec. IV) this reduces to the classic Franz-Keldysh result for the optical absorption in electric field.⁹ Thus, *very long pulses create carriers in Airy eigenstates* with no correlations between neighboring states. However, according to (7), in realistic dc fields the above condition means that the pulse has to be longer than a few tens of picoseconds to be considered “very long” in this sense. Therefore, although we correctly recover the steady-state theory, it is not applicable to femtosecond excitation conditions.

As the excitation pulse becomes shorter, the peaks in curly brackets of (32) grow wider, and at $\tau_p \approx 4\pi\sqrt{\Delta}$ the fast oscillations in (35) will be integrated out [this situation is illustrated in Fig. 2(a)]. Assuming that the pulse is still long enough ($\tau_p \gg 2\pi/\Delta$), and making use of (35) and (30), one can get the following approximation for the intraband DM:

$$n^c(t, \nu) \approx \frac{C e^{i\nu t}}{\sqrt{\Delta}} \cos(\nu\sqrt{\Delta}) e^{-i(\nu|\nu|/4\sqrt{\Delta})} \times \int_{-\infty}^t dt' f(t') f \left[t' - \frac{|\nu|}{2\sqrt{\Delta}} \right] e^{-i\nu t'}. \quad (37)$$

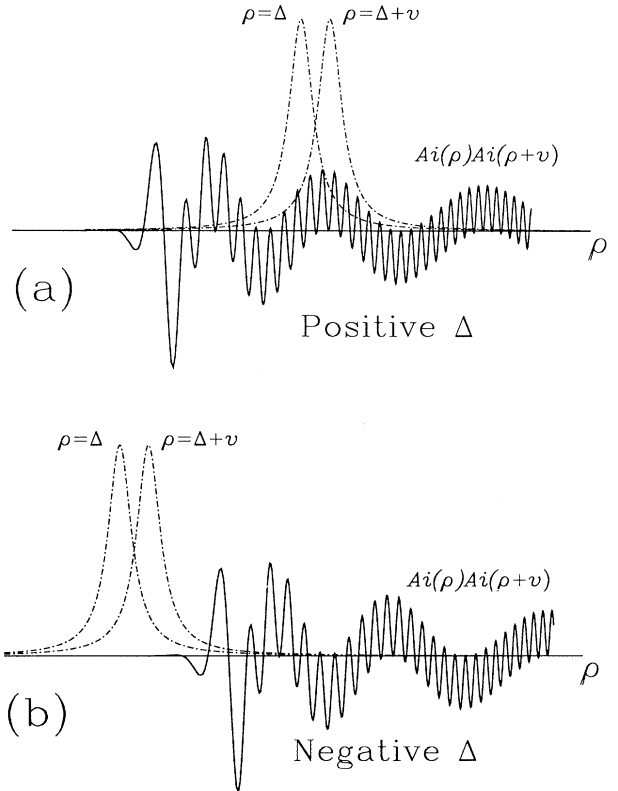


FIG. 2. The structure of the inner integral in Eq. (32). (a) Positive detuning: the Fourier transforms (30) are peaked at $\rho = \Delta$ and $\rho = \Delta + \nu$ where the product of the Airy functions is oscillating according to (35). (b) Negative detuning: the product of Airy functions is exponentially small in the region where the Fourier transforms are peaked, so that the integral is determined by the overlap of the power-law tails (40) with the Airy functions at positive ρ .

The time integral in (37) has a finite width as a function of ν , indicating that the final states are correlated within an energy range of the order of the inverse pulse duration. Physically this reflects the requirements of the time-energy uncertainty principle. Note that within this range the DM is an oscillatory function of ν , and the frequency of oscillations grows with time. To lowest order in ν , the product of the cosine and the exponential in (37) produces oscillations with frequencies $\sqrt{\Delta \pm t}$.

This oscillatory behavior is illustrated in Fig. 3(a), where we plot the real part of the density matrix (32) as a function of the energy ν and time t (since it is even in ν , only the negative part is plotted). Figure 3 is obtained by numerical evaluation of Eq. (32) assuming Gaussian pulse shape for the excitation:

$$f(t) = \exp\left[-\frac{t^2}{\tau_p^2}\right]. \quad (38)$$

[note that the full width at half maximum (FWHM) of such a pulse is $1.665\tau_p$.] Figure 3(b) displays the Fourier transform in energy of the density matrix:

$$n^c(t, \xi) = \int d\nu n^c(t, \nu) e^{-i\xi\nu} \quad (39)$$

versus the argument ξ and time. As is seen from Fig. 3(b), initially the DM oscillates with a single frequency $\sqrt{\Delta}$ as a function of energy, and then at positive times acquires a *two-mode structure* with frequencies $\sqrt{\Delta \pm t}$ that is consistent with our analysis of the asymptotic expression (37).

The other interesting limiting case is for large negative Δ 's. In this case the photons do not have enough energy to cross the band gap. One would expect that at negative detunings there will be no carriers in the bands. However, this is true only after the excitation pulse is over (provided there is no scattering). In fact, excitation below the band gap creates a transient population of carriers that lasts only as long as the excitation pulse.¹² Such carriers are usually referred to as "virtual carriers" as opposed to "real carriers" at positive detunings that stay in the bands *after* the pulse is over.

The concept of virtual carriers can be conveniently expressed in terms of the density-matrix formalism. Consider the density matrix, Eq. (32), at large negative detunings [Fig. 2(b)]. In this case the pulse Fourier transforms in curly brackets will be centered at large negative ρ where the product of Airy functions in (32) is exponentially small. The region $\rho \approx \Delta$ (that gave the greatest contribution at positive detunings) will now give an exponentially small contribution to the integral over ρ (i.e., over

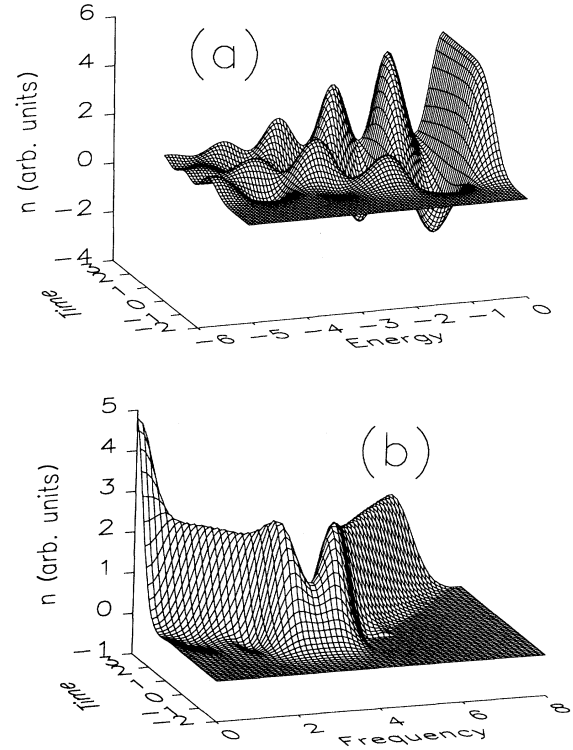


FIG. 3. (a) Intraband density matrix (32) for dimensionless $\Delta=10$ and dimensionless pulse duration $\tau_p=1$. It is about 2π wide as a function of energy, and the oscillatory pattern is well described by the asymptotic formula (37); (b) Fourier transform (39) of the density matrix (a). One sees that after the excitation there are two dominant oscillation frequencies.

the final states). However, the integral itself will not be exponentially small, since the Fourier transforms (30) have slowly decreasing "tails" at large ρ , and the integral is dominated by the overlap of the power-law tails with the Airy functions.

The retarded Fourier transform (30) decreases so slowly at large frequencies because it can be viewed as the usual (from minus to plus infinity) Fourier transform of $f(t')\theta(t-t')$, which is discontinuous at $t=t'$. At large frequencies this discontinuity dominates the integral (30). We can write an asymptotic expression:

$$F_R(t, \Omega)_{\Omega \rightarrow \infty} = -\frac{i}{\Omega} f(t) + \frac{1}{\Omega^2} \frac{df(t)}{dt}. \quad (40)$$

The inner integral in (32) reduces in this case to the simple form

$$\begin{aligned} \int d\rho \text{Ai}(-\rho) \text{Ai}(-\nu-\rho) \{F_R^*(t', \rho-\Delta) + F_R(t', \rho+\nu-\Delta)\} &\approx \int d\rho \text{Ai}(-\rho) \text{Ai}(-\nu-\rho) \left\{ \frac{2f'(t')}{(\rho-\Delta)^2} + if(t') \frac{\nu}{(\rho-\Delta)^2} \right\} \\ &\approx \int_0^\infty d\rho \frac{1}{2\pi\sqrt{\rho}} \cos(\nu\sqrt{\rho}) \left\{ \frac{2f'(t')}{(\rho-\Delta)^2} + if(t') \frac{\nu}{(\rho-\Delta)^2} \right\} \quad (41) \end{aligned}$$

[the integral over negative arguments is neglected since the Airy functions are negligible there, and the product of Airy functions is replaced by (35) at positive arguments]. The real part of (41) can be evaluated:

$$\frac{1}{\pi} \frac{df(t')}{dt'} \int_0^\infty \frac{d\rho}{\sqrt{\rho}} \frac{\cos(\nu\sqrt{\rho})}{(\rho-\Delta)^2} = \frac{1}{2|\Delta|^{3/2}} \frac{df(t')}{dt'} [1 + |\nu|\sqrt{|\Delta|}] e^{-|\nu|\sqrt{|\Delta|}}. \quad (42)$$

As a function of ν , the expression (42) is peaked at $\nu=0$ with the characteristic width $1/\sqrt{|\Delta|} \ll \tau_p$, so we can set $\nu=0$ in the exponent when evaluating the time integral in (32). Taking advantage of the fact that the integrand is proportional to $2f(t')f'(t')=d(f^2(t'))/dt'$, we obtain for the density matrix (32)

$$\text{Ren}^c(t, \nu)_{\Delta \rightarrow -\infty} = \frac{C}{4} \frac{1}{|\Delta|^{3/2}} f^2(t) \times [1 + |\nu|\sqrt{|\Delta|}] e^{-|\nu|\sqrt{|\Delta|}}. \quad (43)$$

Equation (43) clearly shows that the virtual carrier population *adiabatically follows* the instantaneous value of the excitation intensity (in contrast to real carriers whose number is proportional to the time integral of the intensity), so that the virtual carriers disappear after the excitation.

Later on, we will also need the Fourier-transformed DM (39):

$$n^c(t, \xi)_{\Delta \rightarrow -\infty} = C f^2(t) \frac{1}{(|\Delta| + \xi^2)^2}. \quad (44)$$

In Fig. 4 we plot the time-dependent density matrix for $\Delta = -10$ which is obtained by direct numerical evaluation of (32). Figure 4 is in good agreement with the asymptotic result (43).

According to (43), at large negative detunings there is a transient population of virtual carriers proportional to $|\Delta|^{-1.5}$ [note that the number of carriers is given by (43) at $\nu=0$], which follows the square of the excitation envelope. As a function of ν , the width of the density matrix for virtual carriers decreases as $|\Delta|^{-0.5}$, which means that far from the gap virtual carriers become uncorrelated. We will examine the implications of this behavior in the next section.

Thus, in this section we have demonstrated that ultrafast optical excitation in a dc electric field not only creates carries in the bands, but also makes carriers in different states correlated within each band. In the next section we will explore the role these intraband correlations can play in free-electron transport.

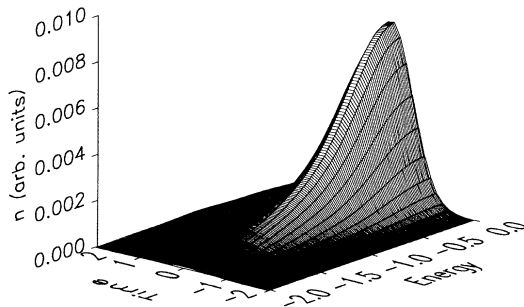


FIG. 4. Intraband density matrix for virtual carriers ($\Delta = -10$ and $\tau_p = 1$).

III. CALCULATION OF THE CHARGE DENSITY AND OTHER OBSERVABLE QUANTITIES

Once the DM is known, we can calculate various observable quantities such as charge and current densities.

A. Charge density

The simplest of observable quantities is particle density, which in terms of the field operators is defined as

$$P(x) = \langle \psi^\dagger(x) \psi(x) \rangle. \quad (45)$$

In the basis of the Airy states (8) and (9) the field operators have the form

$$\psi^\dagger(x, t) = \sum_{\alpha\nu} \psi_\nu^\alpha(x) u^\alpha(x) a_{\alpha\nu}^\dagger(t), \quad (46)$$

where u^α is the periodic part of the Bloch wave functions for band α in the zone center, and the eigenfunctions ψ_ν^α and the operators $a_{\alpha\nu}^\dagger$ have been defined in Eqs. (8), (9), and (13), respectively. Inserting this into (45), we obtain the relation between the particle density and the DM (13):

$$\begin{aligned} P(x) &= \sum_{\alpha\beta\lambda\nu} \psi_\nu^\alpha(x) \psi_\lambda^\beta(x) u^\alpha(x) u^\beta(x) \langle a_{\alpha\nu}^\dagger(t) a_{\beta\lambda}(t) \rangle \\ &= \sum_{\alpha\beta\lambda\nu} \psi_\nu^\alpha(x) \psi_\lambda^\beta(x) u^\alpha(x) u^\beta(x) N_{\nu\lambda}^{\alpha\beta}(t). \end{aligned} \quad (47)$$

The sum over the band indices in (47) contains two interband terms whose contribution to the overall charge density will oscillate with interband frequency in time [cf. Eq. (16)]; this contribution leads to the interband current that interacts with the optical field. However, over times longer than the inverse band gap (about 0.5 fs for GaAs) the interband terms will average to zero. Since we are interested in quantities that vary in time on a much longer time scale of the excitation envelope (typically 100 fs), we can safely leave the interband terms out of (47). Thus, the electron density will read

$$P(x) = \sum_{\alpha\lambda\nu} \psi_\nu^\alpha(x) \psi_\lambda^\alpha(x) n_{\nu\lambda}^\alpha(t), \quad (48)$$

where we have replaced the product of Bloch functions from the same band by unity that is equivalent to unit-cell averaging. Converting to the *hole* density matrix according to (33), we get

$$P(x) = \left[\sum_{\lambda} \psi_\lambda^v(x)^2 \right] + \sum_{\lambda\nu} n_{\nu\lambda}^c(t) \psi_\nu^c \psi_\lambda^c - \sum_{\lambda\nu} n_{\nu\lambda}^h(t) \psi_\nu^v \psi_\lambda^v. \quad (49)$$

The first term here represents the charge density of the filled valence band and is compensated by the positive ion background. It is important to note that the intraband terms contain off-diagonal (in λ, ν) elements of the DM.

Thus, to describe the spatial distribution of particles, we need to know not only the *number* of particles in each eigenstate ($\lambda=\nu$), but also the *correlations* between different eigenstates.

Consider the conduction-band term in more detail:

$$P^c(x) = \sum_{\lambda\nu} n^c(t, \lambda - \nu) \psi_\nu^c(x) \psi_\lambda^c(x) \equiv \sum_{\lambda} \rho_\lambda^c(x, t), \quad (50)$$

where we have introduced

$$\rho_\lambda^c(x, t) \equiv \sum_{\eta} n^c(t, \eta) \psi_\lambda^c(x) \frac{1}{2} \{ \psi_{\lambda+\eta}^c(x) + \psi_{\lambda-\eta}^c(x) \} \quad (51)$$

(the symmetrization is introduced to ensure that this quantity is real). This way we have expressed the total particle density as a sum over energy λ of a set of functions $\rho_\lambda^c(x, t)$ (51) that depend on both coordinate and energy. The quantity (51) is the Wigner function in coordinate-energy representation instead of a more common coordinate-momentum one¹³ (we cannot use the momentum representation because the momentum is no longer a valid quantum number). Its basic property is that the integral over one of its arguments gives the distribution function in the other argument. The energy integral (50) gives the distribution of electrons in space, while integrating (51) over the coordinate yields

$$\begin{aligned} \rho_\lambda^h(x, t) &\equiv \sum_{\eta} n^h(t, \eta) \psi_\lambda^h(x) \frac{1}{2} \{ \psi_{\lambda+\eta}^h(x) + \psi_{\lambda-\eta}^h(x) \} \\ &= \sum_{\eta} n^c(t, \eta) \psi_{\lambda-\Delta}^h(x) \frac{1}{2} \{ \psi_{\lambda-\Delta+\eta}^h(x) + \psi_{\lambda-\Delta-\eta}^h(x) \} \\ &= \sum_{\eta} n^c(t, \eta) \psi_\lambda^h \left[x - \frac{\Delta}{F} \right] \frac{1}{2} \left\{ \psi_{\lambda+\eta}^h \left[x - \frac{\Delta}{F} \right] + \psi_{\lambda-\eta}^h \left[x - \frac{\Delta}{F} \right] \right\} \end{aligned} \quad (54)$$

[the last line of (54) follows from Eq. (33)]. This demonstrates that, for the holes, the coordinate space is shifted by Δ/F against the field, cf. Fig. 1.

By using the density matrix we have plotted in Fig. 3, we can evaluate the Wigner functions (51) and (54) for positive detunings. Figure 5(a) displays the time evolution of the electron Wigner function (51) for the case of optical excitation well above the band edge ($\Delta=10$). The pulse duration is set equal to unity in dimensionless units (5) and (6).

This particular example can be described in purely semiclassical terms. For a given k_\perp and a given Δ , the excitation can be expected to produce an equal number of electrons with the velocities $v_x = \pm \sqrt{2\Delta/m_c}$ corresponding to the excess kinetic energy. As is seen in Fig. 5(a), the localized electronic wave packet created by the optical excitation indeed breaks up into a pair of “particles” that move in opposite directions. One of them is accelerated in the field (and moves out of the frame at later times), while the other decelerates, turns around at the turning point $x=0$, and starts accelerating. Note that in

$$\begin{aligned} \int dx \rho_\lambda^c(x) &= \sum_{\eta} n^c(t, \eta) \frac{1}{2} \left\{ \int dx [\psi_\lambda^c(x) \psi_{\lambda+\eta}^c(x) \right. \\ &\quad \left. + \psi_\lambda^c(x) \psi_{\lambda-\eta}^c(x)] \right\} \\ &= \sum_{\eta} n^c(t, \eta) 2\pi \delta(\eta) = 2\pi n^c(t, (\lambda - \nu) = 0), \end{aligned} \quad (52)$$

which is the number of particles in a given energy state [we have used the orthogonality of the Airy eigenstates (11)].

The translational invariance of the problem manifests itself in the fact that changing all energies by a fixed amount σ is equivalent to shifting the coordinate by σ/F . Because the basis functions (8) and (9) possess this property, the energy dependence of the Wigner function (51) also reduces to a trivial translation in space:

$$\rho_{\lambda+\sigma}^c(x) = \rho_\lambda^c \left[x - \frac{\sigma}{F} \right]. \quad (53)$$

Owing to this translational invariance, we need to know only one function $\rho^c(x, \lambda=0)$ to have a comprehensive description of electron distribution.

In the same way we can introduce the Wigner function for the holes that are connected to the electrons by the optical transition:

addition to the semiclassical particlelike motion we are now able to describe also the size, shape, and location of the electronic wave packets.

This breaking of the initial distribution into two wave packets is closely related to the two-mode behavior of the Fourier-transformed density matrix shown in Fig. 3(b). To demonstrate this, let us rewrite the combination of eigenfunctions that enters (51) in terms of Airy functions (8):

$$\begin{aligned} \frac{1}{2} \psi_{\lambda=0}^c(x) \{ \psi_{0+\nu}^c(x) + \psi_{0-\nu}^c(x) \} \\ = \frac{\beta_c^2}{I_0 \epsilon_0} \text{Ai}(-\beta_c x) \{ \text{Ai}(-\beta_c [x - \nu]) \\ + \text{Ai}(-\beta_c [x + \nu]) \}. \end{aligned} \quad (55)$$

Using the asymptotic expansion (38), for $x \gg 1$ and $|\nu| \ll x$ we can express (55) as

$$\begin{aligned} \frac{1}{2} \psi_{\lambda=0}^c(x) \{ \psi_{0+\nu}^c(x) + \psi_{0-\nu}^c(x) \} \\ \approx \frac{2\beta_c}{\pi I_0 \epsilon_0} \text{Ai}^2(-\beta_c x) \cos(\nu \beta_c \sqrt{\beta_c x}), \end{aligned} \quad (56)$$

so that the Wigner function in this approximation reads

$$\begin{aligned} \rho^c(x,t) &\approx \frac{2\beta_c^2}{\pi l_0} \text{Ai}^2(-\beta_c x) \int d\nu n^2(t,\nu) e^{-i\nu\beta_c\sqrt{\beta_c x}} \\ &= \frac{2\beta_c^2}{\pi l_0} \text{Ai}^2(-\beta_c x) n^c(t, \xi = \beta_c \sqrt{\beta_c x}). \end{aligned} \quad (57)$$

Thus, the Wigner function in the above (semiclassic) limit is just the square of the eigenfunction modulated by an envelope that reproduces the time dependence of the

Fourier-transformed DM (39). The two peaks at $\xi = \sqrt{\Delta} \pm t$ in the latter quantity give rise to two “particles” localized at

$$\begin{aligned} X_{\pm} &= \frac{1}{\beta_c^3} (\Delta \pm 2t\sqrt{\Delta} + t^2) \\ &= \frac{m_r}{m_c} \frac{\Delta}{F} \pm t \left[\frac{2\Delta}{m_r} \frac{m_r}{m_c} \right]^{1/2} + \frac{F}{m_c} \frac{t^2}{2} \end{aligned} \quad (58)$$

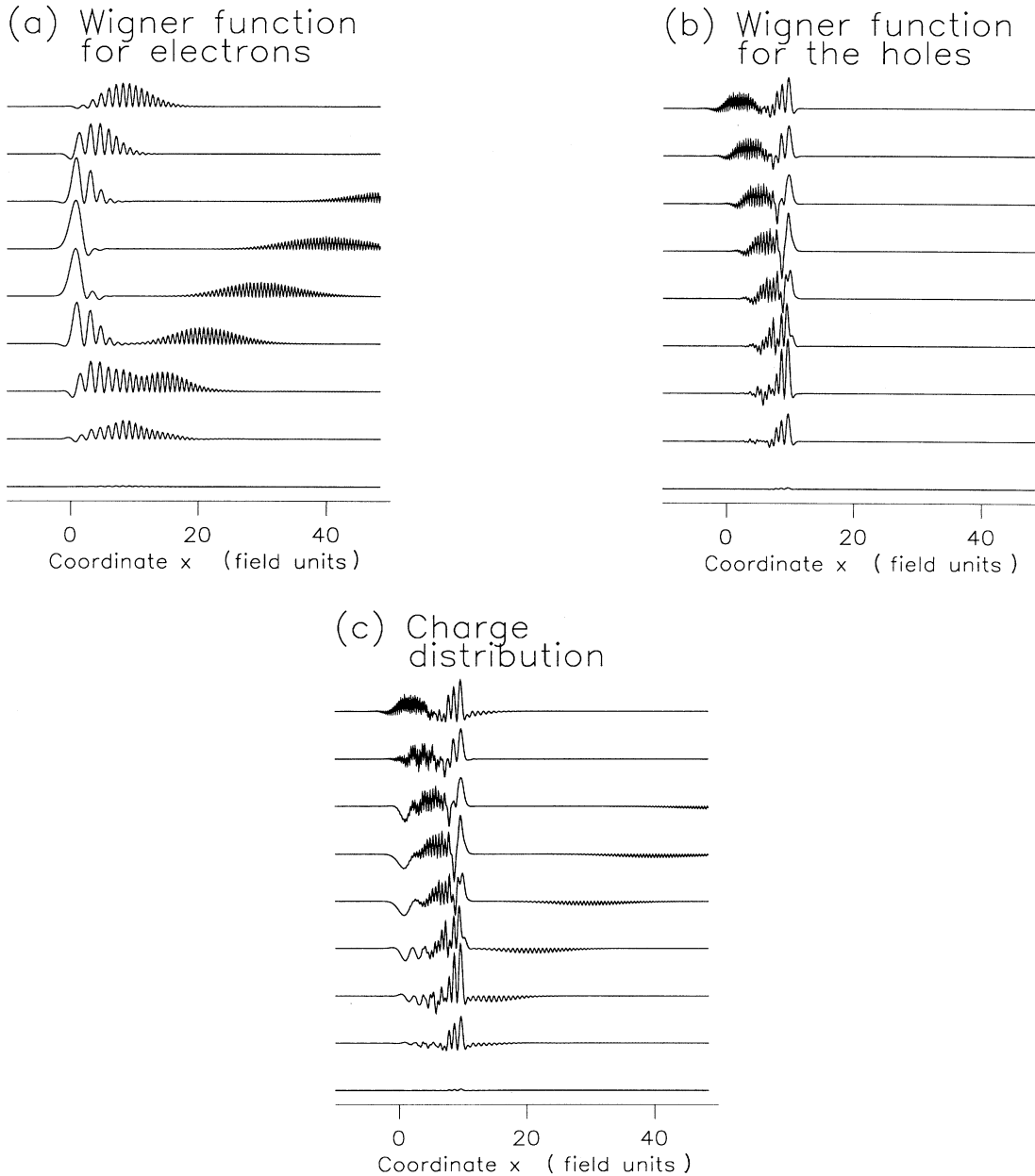


FIG. 5. (a) Wigner function for electrons (51) at different times during the excitation ranging from -1 (bottom trace) to 7 (top) pulse durations. Excitation parameters are the same as in Fig. 3. Electrons are created by light as localized wave packets that later break up into two particles going in opposite directions. (b) Wigner function (54) for the holes. Note that there are regions where it goes negative. (c) Charge density (59). Since electrons and holes are created basically around the same point in space, initially there seems to be no net dipole moment.

[we have switched over to dimensional units according to (5) and (6)].

The meaning of (58) is quite transparent: the light creates electrons at a distance $(m_r/m_c)(\Delta/F)$ from the turning point with initial velocities given by the factor beside t in (58) (which is just enough for the particle going against the field to reach the turning point), and then both particles move with the acceleration F/m_c , just as one would expect semiclassically. It is interesting to note that the holes are initially localized around $\Delta/F - (m_r/m_h)\Delta/F = (\Delta/F)(m_r/m_e)$. This is exactly where the electrons are created. Thus, the Δ/F shift in the coordinate space of the holes [Eq. (54)] does *not* mean that electron and hole wave packets are separated by this distance; instead, for the real carriers our analysis corroborates the intuitive assumption that both electrons and holes have to be created at the same point in space.

As the duration of the excitation pulse increases, the Fourier-transformed DM becomes broader, so that the wave packets in Fig. 5(a) become wider in space. Eventually, they will fill the entire sample. This corresponds to the steady-state, cw limit of Franz-Keldysh theory.⁹ However, for short pulses, the transient localization evident in Fig. 5(a) will have important consequences for the photocurrent calculation.

In Fig. 5(b) we present the time dependence of the hole Wigner function (54). Because the holes are assumed to be ten times heavier than electrons, the relevant range of coordinates is no longer much greater than the energy spread of the density matrix (said another way, to the heavier holes the pulse effectively seems much shorter), so the above asymptotic analysis breaks down. As a result, it is harder to interpret Fig. 5(b) semiclassically, especially in the vicinity of the turning point. An obvious manifestation of the quantum nature of hole transport in this example is the presence of negative peaks in the Wigner function in Fig. 5(b). In semiclassics the Wigner function can be considered a distribution function and is therefore positive definite, which is not necessarily true in the general quantum case. Finally, in Fig. 5(c) we plot the charge density, defined as

$$\rho_{\lambda=0}(x) = \rho^h(x) - \rho^e(x). \quad (59)$$

Note that since the electron and hole distributions are centered around the same point in space, the charge density does not seem to be polarized by the dc field. We see that even though the polarization of extended eigenstates is infinite (or proportional to the sample size in a finite-size sample), the transient localization of the real carriers causes them to have a finite (and actually rather small) dipole moment in this case.

The behavior of the virtual carriers turns out to be completely different in this respect. As illustrated by Fig. 6, their pair charge density is visibly polarized: the holes are created much further down the field than the electrons, and the Wigner functions for both electrons and holes are stretched by the dc field. Since we know the asymptotic form of the Fourier-transformed DM in the limit of large negative detunings (44), we can obtain an expression for the Wigner distribution of virtual conduction electrons by making use of (57):

Virtual carriers

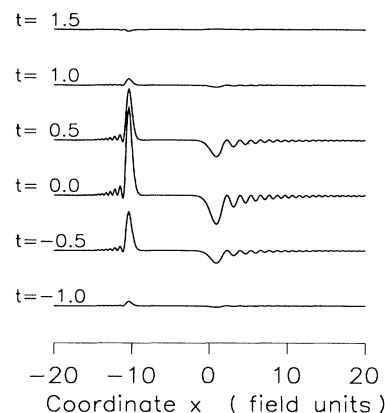


FIG. 6. Charge density (59) for virtual carriers. Excitation parameters are that of Fig. 4. The carriers are visibly stretched by the dc field and show no signs of classical motion.

$$\rho^c(t, x)_{\Delta \rightarrow -\infty} = \frac{2\beta_c^2}{\pi l_0} \text{Ai}^2(-\beta_c x) C f^2(t) \frac{1}{(|\Delta| + \beta_c^3 x)^2}. \quad (60)$$

With growing $|\Delta|$ the electron Wigner function becomes increasingly delocalized and approaches the square of the corresponding eigenfunction. Thus, the virtual carriers differ from real carriers not only in the peculiar temporal dependence of their density,¹² but also in the way their charge is distributed in space.

B. Dipole moment and photocurrent

We can calculate the current using its real-space definition as a time derivative of the polarization. This approach seems natural for the situation under study, since here we do not have any current flowing in and out of the sample, but instead have a redistribution of electrons within the depletion layer under the action of the laser pulse.

From the real-space point of view, the basic process is the separation of electrons and holes in the dc field. As charges separate, the medium acquires a dipole moment per unit volume equal to the dielectric polarization. This dipole moment is time dependent, and its time derivative gives the current density.

Let us consider an interval of unit length inside the semiconductor. We can calculate the charge distribution over this interval by integrating pair charge density $\rho_\lambda(x)$ (59) over a finite range of λ [cf. (49)] from certain λ_0 to $\lambda_0 + F$ (because the energy changes by F over a unit length), and then determine the dipole moment of this distribution of charges, $D(t)$. However, since the pair density (59) does not depend on λ except for the trivial shift in space (53), the result will simply be the dipole moment of a single pair $d(t)$ multiplied by the number of states per unit interval, which is again equal to F :

$$\begin{aligned}
D(t) &= \int_{-\infty}^{+\infty} dx x \int_{\lambda_0}^{\lambda_0+F} d\lambda \rho_\lambda(x,t) \\
&= \int_{\lambda_0}^{\lambda_0+F} d\lambda \int_{-\infty}^{+\infty} dx x \rho_\lambda(x,t) \\
&= \int_{\lambda_0}^{\lambda_0+F} d\lambda d_\lambda(t) = F d_{\lambda=0}(t), \quad (61)
\end{aligned}$$

(due to the overall neutrality of the pair, its dipole moment $d_\lambda(t)$ is independent of its location in space, i.e., of λ). Note that this approach is exactly equivalent to the usual way of calculating the polarization in conventional dielectrics by multiplying the dipole moment of each molecule by the number of molecules. Indeed, (61) is a product of the dipole moment of an electron-hole pair ("molecule") and the number of pairs per unit length F .

If the pairs were delocalized, this calculation would give an infinite dipole moment. For our localized pairs the dipole moment will tend to infinity as particles separate in the dc field, but for any finite time it will be finite. This shows that taking the steady-state limit^{4,6} in fact leaves out all the essential physics of the problem, namely, the process of creation and separation of charge carriers during and immediately after the photoexcitation.

Let us now consider the expression for the dipole moment of the pair at $\lambda=0$:

$$d_\lambda(t) = \int_{-\infty}^{+\infty} dx x \rho_\lambda(x,t) = d_\lambda^c(t) + d_\lambda^h(t), \quad (62)$$

where we have split the pair density (59) into its electron and hole components. Let us rewrite the dipole moment of electrons using the representation (50):

$$d_\lambda^c(t) = \int d\eta x dx n^c(t,\eta) \psi_\lambda^c(x) \times \frac{1}{2} \{ \psi_{\lambda+\eta}^c(x) + \psi_{\lambda-\eta}^c(x) \}. \quad (63)$$

At any given η the integrand diverges as a function of x , so that for an electron that occupies one of the eigen-

states the dipole moment would be infinite. However, as we have shown, the density matrix is in fact nonzero in a certain range of energies, so that after the integration over η the oscillations in Airy functions will cancel each other at large x , giving a finite dipole moment that results from the above discussed transient localization of particles.

The dipole moment (63) can be conveniently expressed through the Fourier transform (39) of the density matrix. By using the expression (8) for the eigenfunctions along with the integral representation (10) for the Airy function, after some algebra we get for (63)

$$d_{\lambda=0}^c(t) = \frac{l_0}{\beta_c^3} \int d\xi n^c(t,\xi) \xi^2. \quad (64)$$

In the same way we obtain for the hole dipole moment

$$d_{\lambda=0}^h(t) = \frac{l_0}{\beta_h^3} \int d\xi n^c(t,\xi) \xi^2 - l_0 \Delta \int d\xi n^c(t,\xi). \quad (65)$$

Thus, the pair dipole moment takes on the form

$$d_{\lambda=0}(t) = l_0 \int d\xi n^c(t,\xi) \xi^2 - l_0 \Delta \int d\xi n^c(t,\xi). \quad (66)$$

Note that the pair moment turns out to be independent of the electron-hole mass ratio [we have used the definition $\beta_{c,h} = (m_{c,h}/m_r)^{1/3}$ to obtain (66)].

The second integral in (66) is just $2\pi n^c(t,\eta=0)$, which is the total number of particles [cf. (52)], so that the second term simply accounts for the fact that the hole distribution is shifted by Δ with respect to that of the electrons (see Fig. 1).

At positive detunings we can also make some general statements about the first term, since we know the structure of the Fourier-transformed DM (39) [see Fig. 3(b)]. If we replace the two peaks of (39) at $\sqrt{\Delta} \pm t$ by two δ functions (which is the same as assuming that the two wave packets in Fig. 5 are very tightly localized), then the dipole moment (66) can be estimated as

$$\begin{aligned}
d^{\text{cl}}(t) &\approx l_0 \int d\xi n_0 \xi^2 \left\{ \frac{1}{2} \delta(\sqrt{\Delta} + t) + \frac{1}{2} \delta(\sqrt{\Delta} - t) \right\} - l_0 \int d\xi n_0 \Delta \left\{ \frac{1}{2} \delta(\sqrt{\Delta} + t) + \frac{1}{2} \delta(\sqrt{\Delta} - t) \right\} \\
&= (l_0 n_0) \times \left[\frac{1}{2} (\sqrt{\Delta} + t)^2 + \frac{1}{2} (\sqrt{\Delta} - t)^2 - \Delta \right] = l_0 n^c(t,\eta=0) t^2. \quad (67)
\end{aligned}$$

This corresponds to a semiclassical situation when well-defined particles move in the dc field with constant acceleration. Note that the oscillations in the DM with the frequency $\sqrt{\Delta}$ tend to compensate the displacement contribution given by the second term in (66). This is in line with the observation made after Eq. (58) that excitation above the band gap creates electrons and holes around the same point in space. However, this cancellation occurs in leading order only. The Fourier-transformed DM is not exactly a combination of two δ functions [and it only has this two-mode structure at sufficiently large times after the excitation; see Fig. 3(b)]. In general, in addition to the semiclassical (transport) terms (67), the total dipole moment (66) will contain additional (displacement) terms.

To gain further insight into the evolution of the pair dipole moment (66) we have to treat it more rigorously. Using the well-known properties of the Fourier transform, (66) can be rewritten as

$$d_{\lambda=0}(t) = 2\pi l_0 \left[\left[\frac{\partial^2 n^c(t,\eta)}{\partial \eta^2} \right]_{\eta=0} - \Delta n^c(t,\eta=0) \right]. \quad (68)$$

The second derivative of the density matrix that enters (68) can be evaluated by differentiating the expression (32). After some cumbersome but straightforward transformations, we arrive at the following result for d :

$$\begin{aligned}
d_{\lambda=0}(t) &= \frac{2m_0 l_0}{\pi \hbar^2} \frac{|\mu_{cv}|^2 E_0^2}{F^2} - \left\{ \int_{-\infty}^t dt' (t-t')^2 f(t') \int d\rho \text{Ai}^2(-\rho) 2 \text{Re} F_R(t', \rho - \Delta) \right. \\
&\quad + \int_{-\infty}^t dt' f(t') \int d\rho (\rho - \Delta) \text{Ai}^2(-\rho) 2 \text{Re} F_R(t', \rho - \Delta) \\
&\quad \left. - t \int_{-\infty}^t dt' f(t') \int d\rho \text{Ai}^2(-\rho) 2 \frac{\partial}{\partial \rho} \text{Im} F_R(t', \rho - \Delta) \right\} \\
&= C_d \{d_1 + d_2 + d_3\} .
\end{aligned} \tag{69}$$

The first term in (69) is the semiclassical result for the dipole moment. Indeed, let us rewrite it using (32):

$$d_1(t) = l_0 \int_{-\infty}^t dt' (t-t')^2 2\pi \frac{\partial n^c(t', \eta=0)}{\partial t'} . \tag{70}$$

This expression can be easily understood in semiclassical terms: this is the dipole moment of the classical particles that are being created by the excitation pulse. The derivative in (70) is the generation rate, and Eq. (70) simply means that each of the particles created between t' and $t'+dt'$ will have gained a dipole moment $l_0(t-t')^2$ by the time t . The integral in (64) just sums up the contributions of all such groups of particles created at different times in the past.

The remaining two terms in (69) represent quantum corrections to the classical result (70). We will refer to them as “displacement terms” to distinguish them from the “transport” term (70).

In the next section we will study the relative importance of these terms numerically. However, for virtual carriers we can also obtain an analytic result for the dipole moment either by evaluating (69), or by directly integrating the charge density (60):

$$d(t)_{\Delta \rightarrow -\infty} = \frac{Cl_0}{4\sqrt{|\Delta|}} f^2(t) . \tag{71}$$

Note that (71) decreases very slowly as the frequency is tuned away from the band gap.

To summarize, the results of this section allow us to calculate time-dependent density of photoexcited particles and predict the resulting changes in the dielectric polarization of the medium. Based on these results, in the next section we will evaluate experimentally relevant quantities and discuss some unusual features that arise under femtosecond excitation conditions.

IV. RESULTS AND DISCUSSION

In the preceding sections, we considered the behavior of carriers for a fixed perpendicular momentum k_{\perp} . However, in general, all states with different k_{\perp} will contribute to the quantities of interest, so we have to carry out the summation over all perpendicular momenta. Because we have neglected Coulomb effects and relaxation processes that could couple states with different k_{\perp} , this summation is simple.

A. Density of photoexcited carriers

The first quantity we want to calculate is the total density of the photoexcited particles. This is proportional to the optical absorption. Equation (52) states that the number of particles occupying a given eigenstate is given by the intraband density matrix at coincident energy arguments. This quantity implicitly depends on k_{\perp} , since Δ is different for different perpendicular momentum states:

$$\Delta \equiv \hbar\omega - E_g^{\perp} = \hbar\omega - E_g - \frac{\hbar^2 k_{\perp}^2}{2m_0} = \Delta_0 - \frac{\hbar^2 k_{\perp}^2}{2m_0} . \tag{72}$$

Here we define $\Delta_0 \equiv \hbar\omega - E_g$ to be the “real” detuning.

To get the volume density of particles, we have to sum up (52) over all eigenstates. There are F eigenstates per unit length in the field direction, so the summation over energy index λ is performed simply by multiplying (52) by the dc field, while the summation over perpendicular momentum quantum numbers is, according to (72), equivalent to integration over Δ :

$$\begin{aligned}
&2 \int d^2 k_{\perp} F(\Delta) \\
&= \int_{-\infty}^{\Delta_0} \frac{2m_0}{\hbar^2} d\Delta F(\Delta) = \frac{2m_0}{\hbar^2} \epsilon_0 \int_{-\infty}^{\Delta_0} d\Delta F(\Delta) .
\end{aligned} \tag{73}$$

Here we have switched to integration over the dimensionless energy; the factor of 2 accounts for the spin. Thus, the total number of particles is

$$\begin{aligned}
N(t) &= F \frac{2m_0}{\hbar^2} \epsilon_0 \int_{-\infty}^{\Delta_0} 2\pi n^c(t, \nu=0) d\Delta \\
&= C_N \int_{-\infty}^{\Delta_0} \int_{-\infty}^t dt' f(t') \int d\rho \text{Ai}^2(-\rho) \\
&\quad \times 2 \text{Re} F_R(t', \rho - \Delta) .
\end{aligned} \tag{74}$$

The prefactor in (74) is given by

$$C_N = \frac{4\epsilon_0}{\pi} \left[\frac{m_0}{\hbar^2} \right]^2 \frac{|\mu_{cv}|^2 E_0^2}{F} = 1.57 \times 10^{15} \text{ cm}^{-3} I F^{-1/3} . \tag{75}$$

We have used GaAs parameters ($m_r=0.061$, $\mu_{cv}=0.7$ nm) to get the numerical factor. The numerical factors are calculated for dc field F measured in kV/cm and the optical intensity I in MW/cm².

The power-law dependence of the density prefactor C_N (75) on the dc field F does not mean that the density will

have the same F dependence since the integrals in (74) also implicitly depend on the dc field through our field-dependent units of measurements (5) and (6). To see how this implicit field dependence compensates the power-law prefactor, let us consider (74) in the limit of long pulses, where we can rewrite the integrals as

$$\begin{aligned} & \int_{-\infty}^{\Delta_0} \int_{-\infty}^t dt' f(t') \int d\rho \text{Ai}^2(-\rho) 2 \text{Re} F_R(t', \rho - \Delta) \\ & \approx \frac{1}{\pi} \int_{-\infty}^{\Delta_0} d\Delta \text{Ai}^2(-\Delta) \int_{-\infty}^t dt' f^2(t') \\ & \approx \frac{1}{\pi^2} \sqrt{\Delta_0} \int_{-\infty}^t dt' f^2(t'). \end{aligned} \quad (76)$$

The integral of Airy function squared was taken using the square-root asymptotics (35). In this equation Δ is dimensionless, and as the energy unit (6) $\varepsilon_0 = (\hbar^2/2m_r)^{1/3} F^{2/3}$ increases with growing field, dimensionless detuning will decrease, so that the factor $\sqrt{\Delta_0}$ in (76) will in fact scale with the field as $F^{-1/3}$. Likewise, the time integral also depends on the field, because with increasing field the time unit (6) diminishes, making the pulse longer in dimensionless units. Thus, the time integral will scale with the field as $1/\tau_0 \propto F^{2/3}$, so that on the whole (75) scales with the field as $F^{1/3}$, exactly compensating the field dependence of the prefactor.

Figure 7 illustrates this behavior. The particle density as a function of detuning is largely field independent, although at higher fields Franz-Keldysh oscillations appear on top of the square-root density of states. The same is true for virtual carriers, whose density evolution is illustrated in Fig. 8. According to (43), for the virtual carriers the integral over Δ in (74) will scale as $1/\sqrt{|\Delta|/\varepsilon_0} \propto F^{1/3}$, which again cancels the field dependence of the prefactor.

B. Dielectric polarization

Applying a similar treatment to our result for the dipole moment (69), we get the following expression for the

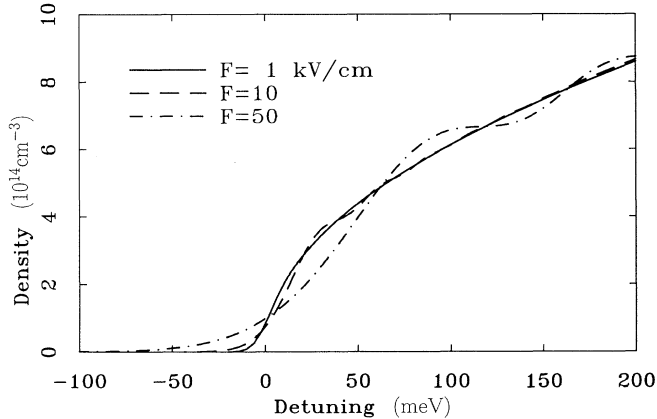


FIG. 7. Particle density (74) at $t = 300$ fs as a function of detuning in different dc fields. Here and in the subsequent figures we assume a pulse of 100-fs duration with the peak intensity of 0.1 MW/cm^2 and evaluate (74) numerically. Growing dc field just redistributes spectral weight (Franz-Keldysh oscillations), so that the density stays practically constant.

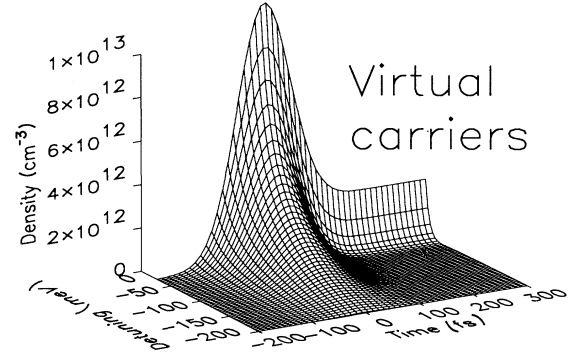


FIG. 8. Time dependence of virtual carrier density obtained by numerical evaluation of (74) at negative detunings. Note that as the excitation frequency is tuned closer to the band gap, the density increases sharply and does not go to zero after the pulse is over, so that the transition from virtual to real carriers is rather abrupt.

dielectric polarization \mathbf{P} which is the dipole moment of a unit volume:

$$\mathbf{P}(t) = C_P \int_{-\infty}^{\Delta_0} d\Delta (d_1 + d_2 + d_3), \quad (77)$$

where d_i denote the dimensionless integrals in (69), and

$$\begin{aligned} C_P &= C_N l_0 = \frac{4l_0^2}{\pi} \left(\frac{m_0}{\hbar^2} \right)^2 |\mu_{cv}|^2 E_0^2 \\ &= 9.34 \times 10^{-10} \text{ C/cm}^2 \text{IF}^{-2/3} \end{aligned} \quad (78)$$

is the same prefactor (75) multiplied by the length unit l_0 .

As seen from Eq. (70), the first (transport) term of (77) will scale with the field as $1/\tau_0^3 \sqrt{\varepsilon_0} \propto F^{5/3}$. This gives a linear dc field dependence with the prefactor (78). It is instructive to rewrite (70) in dimensional units:

$$\mathbf{P}_{\text{tr}}(t) = \frac{l_0}{\tau_0^2} \int dt' (t-t')^2 \frac{\partial N}{\partial t'} = \int dt' \frac{F}{2m_0} (t-t')^2 \frac{\partial N}{\partial t'}, \quad (79)$$

which makes the physical interpretation of this term clear: it describes acceleration of classical particles in the dc field and is therefore linear in F .

The remaining terms in the expression (69) for the pair dipole moment have somewhat different structure that leads to a different field dependence. Unfortunately, in general the last two integrals in (69) can be shown to depend on the particular functional form of the envelope f , so that we are unable to derive an asymptotic expression for these terms at positive Δ , although simple estimates show them to be much smaller than the transport term (70) for pulses with the dimensionless duration greater than unity. However, at large negative Δ the integrals in (79) can be evaluated by replacing the retarded Fourier transform with its power-law asymptotics (40), which results in Eq. (71) for the dipole moment of virtual pairs.

Because (71) decreases only as $|\Delta|^{-1/2}$, the summation over perpendicular momentum (73) will give a divergent result. Although there are fewer and fewer virtual pairs

for high k_{\perp} , the pairs become increasingly delocalized with growing $|\Delta|$ [according to Eq. (60), each virtual pair carries a dipole moment proportional to $|\Delta|$]. If we impose a high- δ cutoff Δ_m in the integral (77), the polarization caused by virtual carriers can be expressed as

$$\mathbf{P}_{\text{dis}}(t) = \frac{C_P}{2} f^2(t) \{ \sqrt{\Delta_m} - \sqrt{\Delta_0} \}. \quad (80)$$

The divergence of this quantity is a consequence of our simplified description of the band structure. At high k_{\perp} it can no longer be described by our simple parabolic model with constant interband matrix element. As is often the case with calculations of nonlinear optical susceptibilities, we need to take into account the decrease in the matrix element and changes in dispersion relations for the particles as k_{\perp} moves away from the zone center. However, we can view the cutoff procedure as a way to account for nonresonant contributions to (80) by replacing them with a detuning-independent constant.

The cutoff may also be imposed by purely geometrical constraints. In a finite-size sample the width of the pair charge distribution cannot increase indefinitely, and the maximum dipole moment per pair will be limited by the size of the sample (in a bulk sample the cutoff distance will be the depletion layer thickness or the absorption length). However, recent work on conjugated polymers¹⁴ suggests that the Coulomb attraction between the electron and the hole might be the most important factor that limits their separation. Since the treatment of the excitonic effects is beyond the scope of the present work, here it seems reasonable to cut off the integral by the condition that the separation between pairs (Δl_0 , cf. Fig. 6) does not exceed a certain critical length L . This will give us the following expression for the virtual polarization (80):

$$\mathbf{P}_{\text{dis}}(t) = \frac{1}{2} C_P f^2(t) \left\{ \left[\frac{L}{l_0} \right]^{1/2} - \sqrt{\Delta_0} \right\}. \quad (81)$$

Here we will adopt this geometrical interpretation and consider the cutoff length as a fitting parameter. Realistic values of L are of the order of a few micrometers, so that for dc fields in kV/cm range [with the length unit (5) of the order of a few tens of nanometers] Δ_m will be of the order of a few tens (e.g., for $L = 1 \mu\text{m}$ and $F = 1 \text{ kV/cm}$, $\Delta_m = 27$).

As a function of detuning, (81) is zero at $\Delta_0 = \Delta_m$, then it grows as the excitation frequency approaches the band gap, where it reaches the maximum value

$$\mathbf{P}_{\text{dis}}(t) = \frac{1}{2} C_P f^2(t) \left[\frac{L}{l_0} \right]^{1/2} \quad (82)$$

and stays practically constant at positive detunings (because for real carriers the displacement term is small).

This behavior is illustrated by Fig. 9, where we plot the total polarization (75) and its two constituent parts: while the transport contribution to the polarization [Fig. 9(b)] grows quadratically with time elapsed after the excitation according to (74), the displacement contribution [Fig. 9(c)] is essentially present only during the excita-

tion, and follows the above described pattern as a function of detuning.

The most striking feature of (82) is that it depends on the dc field in a very unexpected way. Using the expressions (5) for l_0 and (78) for the prefactor, it is easy to see that (82) is proportional to $F^{-2/3} F^{1/6} = 1/\sqrt{F}$, which means that the displacement contribution *actually decreases with increasing dc field*. The peak value of (82) at $t = 0$ is

$$\mathbf{P}_{\text{dis}}^m(t) = \frac{1}{2} C_P \left[\frac{L}{l_0} \right]^{1/2} = 2.41 \times 10^{-9} \text{ C/cm}^2 F^{-1/2}. \quad (83)$$

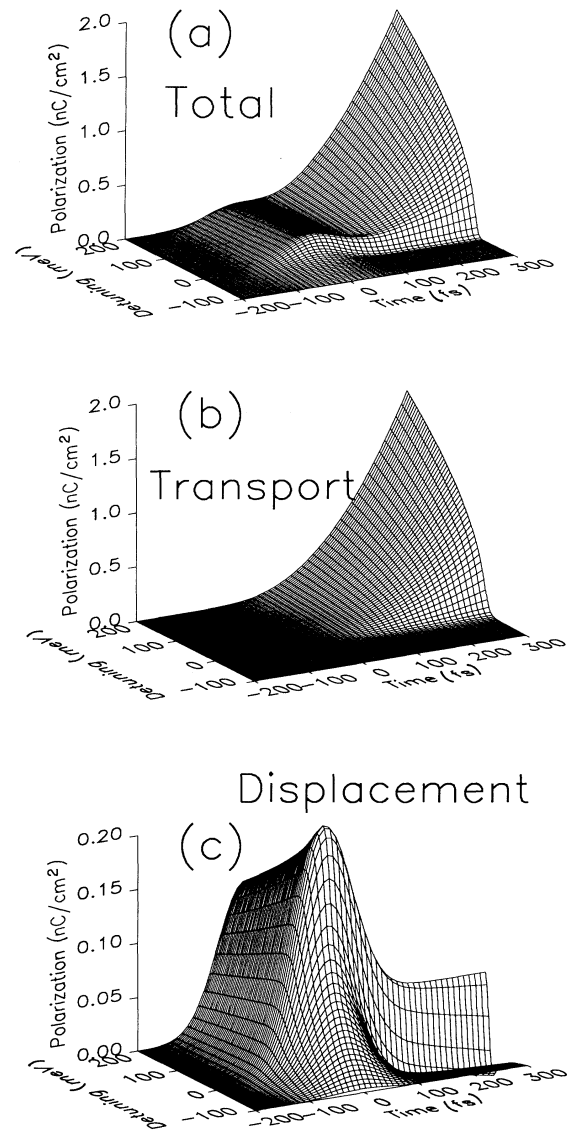


FIG. 9. (a) Total polarization (77) for $F = 1 \text{ kV/cm}$ in nanoCoulombs/cm² for excitation parameters of Fig. 7. The cutoff length has been set to $1 \mu\text{m}$; (b) transport contribution to the polarization; (c) displacement contribution.

Qualitatively, the decrease of the polarization with growing dc field can be explained by the fact that stronger fields will tilt the bands more, so that in absolute units the electron-hole separation Δ/F decreases with the field (cf. Fig. 1). Unlike atomic and molecular systems where the charge separation in the dc field is limited by the dimensions of the particles, electrons in a semiconductor have an additional freedom to choose the separation distance. The dc field not only pulls the particles apart but also restructures the electronic eigenstates, and it turns out that for virtual carriers the net result is the decreasing pair dipole moment with increasing field.

It is a general prediction of the perturbation theory that in weak fields the polarization grows linearly with the field. However, the perturbation treatment of the dc field breaks down at very low fields. The general criterion is that the magnitude of the perturbation FL (which is the potential drop across the sample of length L) should not exceed the interlevel spacing $\hbar^2/2m_r L^2$. For, e.g., a 1- μm sample this means that fields above 0.1 V/cm cannot be treated perturbatively. Note that this criterion of applicability for the perturbation theory can be rewritten as $L \ll l_0$, which is exactly the opposite of what is required for our approach [see the discussion after Eq. (12)]. Therefore, at very low fields the polarization can be expected to grow linearly in the dc field with a very large polarizability (proportional to the sample size), and in the field range where the perturbative treatment breaks down this linear growth turns into the decreasing dependence predicted by our nonperturbative approach that should work as long as the dimensionless cutoff parameter $\Delta_m \equiv L/l_0$ is much greater than unity.

C. Photocurrent

The unusual field dependence of the displacement term in polarization is evident in Fig. 10, where we plot the time derivative of the polarization (i.e., the photocurrent) at different dc fields. For a relatively high field value of 10 kV/cm [Fig. 10(a)] the photocurrent is completely dominated by the transport term (79)

$$\mathbf{j}_{\text{tr}}(t) = \frac{d\mathbf{P}_{\text{tr}}}{dt} = \int_{-\infty}^t dt' \frac{F}{m_0} (t-t') \frac{\partial N}{\partial t'}, \quad (84)$$

which grows linearly with time after the excitation and follows the detuning dependence of the density (cf. Fig. 7). Note that in reality this linear growth will be eventually (at times of the order of the momentum relaxation times that we assume to be much longer than the pulse duration) arrested by scattering processes. The displacement term is responsible for a small feature around $t=0$ at negative detunings, but at positive detunings it is negligible compared to the transport term.

Decreasing the field ten times to 1 kV/cm [Fig. 10(b)] makes the transport term ten times smaller while the displacement term grows by $\sqrt{10}$, so that they become quite comparable. Note that the photocurrent first flows along the field, then reverses its direction near $t=0$, and then flows along the field again after the transport current begins to dominate at later times.

Finally, Fig. 10(c) shows an example where the dis-

placement current dominates completely. This case approaches the limits of applicability of our analysis. At positive times the photocurrent actually flows *against the field* as virtual carriers are annihilated.

Thus, we see that as the dc field decreases, the photocurrent experiences a gradual crossover from semiclassical transport-dominated behavior to a quantum regime where displacement current dominates. As a result, not only does its magnitude vary nonlinearly with the field,

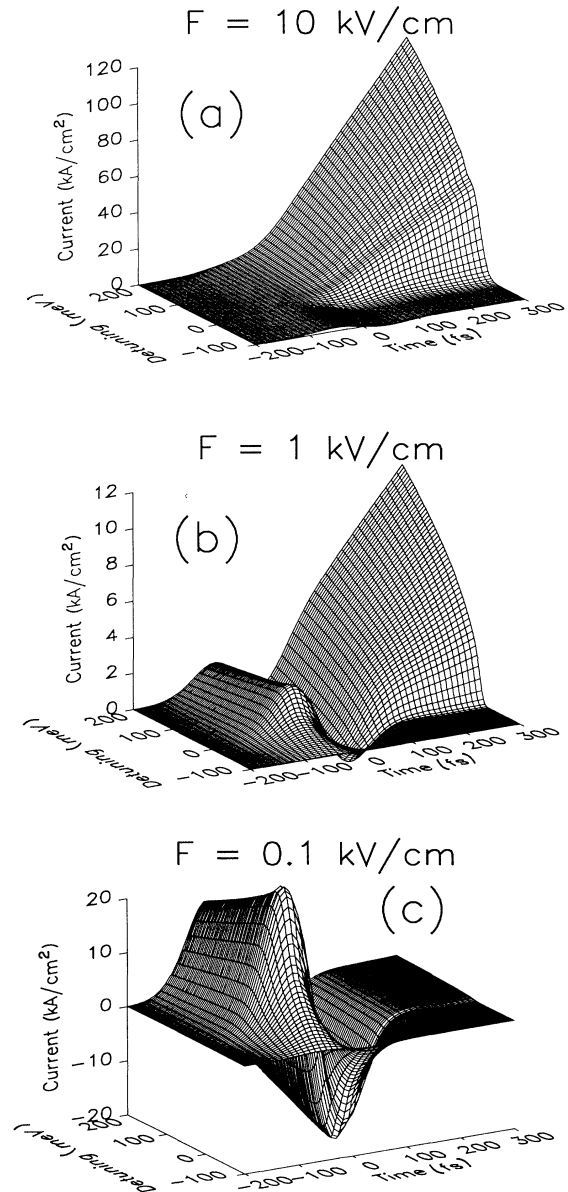


FIG. 10. (a) Photocurrent at a high dc field of 10 kV/cm for the same excitation parameters. It follows the semiclassical expression (84) very well; (b) photocurrent at a lower field cannot be viewed as transport current alone; (c) at 0.1 kV/cm the photocurrent is completely dominated by the displacement feature. The cutoff distance was increased from 1 to 3 μm for (c), so the field dependence of the displacement current does not quite match Eq. (83).

but also its temporal dependence undergoes dramatic changes.

D. Terahertz radiation signal

To study this crossover phenomenon in more detail, let us examine the behavior of time derivative of the photocurrent. This quantity is more relevant experimentally, since in terahertz radiation experiments¹⁻⁵ the signal is believed to be proportional to the derivative of the current.

Optical excitation produces time-dependent current in the medium which, according to Maxwell's equations, should emit electromagnetic radiation. Assuming that the excitation pulse is incident on the sample at an angle ϕ_0 , that the penetration depth z is much smaller than the spot size S , and that the detector is located at an angle ϕ and at a distance r_0 , by a direct solution of Maxwell's equations one can get the following result for the electric field of the radiated signal at the detector:

$$E(r_0, t) = \frac{\sin\phi}{4\pi\epsilon\epsilon_0 c} \frac{S z}{r_0} \frac{\left[\mathbf{j} \left[t' + \frac{S}{c} \Delta\phi \right] - \mathbf{j} \left[t' - \frac{S}{c} \Delta\phi \right] \right]}{\Delta\phi}$$

$$\approx \frac{\sin\phi_0}{\phi \rightarrow \phi_0} \frac{S^2 z}{4\pi\epsilon\epsilon_0 c^2} \frac{d\mathbf{j}(t')}{dt}, \quad (85)$$

where $t' = t - r_0/c$ and $\Delta\phi = \cos\phi - \cos\phi_0$. At small $\Delta\phi$ this indeed becomes proportional to the derivative of the current density.

$$E_{\text{tr}}(t) \propto \frac{d^2}{dt^2} \mathbf{P}_{\text{tr}}(t) = \frac{l_0}{\tau_0^2} \frac{d^2}{dt^2} \int_{-\infty}^t dt' (t-t')^2 \frac{\partial N}{\partial t'} = \int dt' \frac{F}{m_0} \frac{\partial N}{\partial t'} = \frac{F}{m_0} N(t), \quad (86)$$

which is positive and grows with Δ . As a result, at sufficiently high positive detuning the transport contribution compensates the displacement one, and the signal changes sign at $t=0$.

This crossover effect is illustrated in Fig. 12, where we plot the signal versus detuning at $t=0$. As the dc field grows the crossover point moves closer to the band edge.

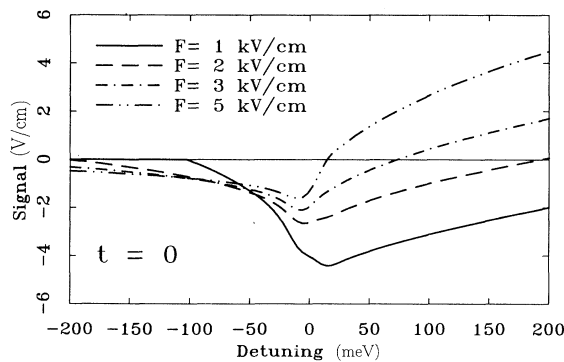


FIG. 12. The signal at the center of the pulse vs detuning. It experiences a sign reversal at some critical detuning that decreases with the field.

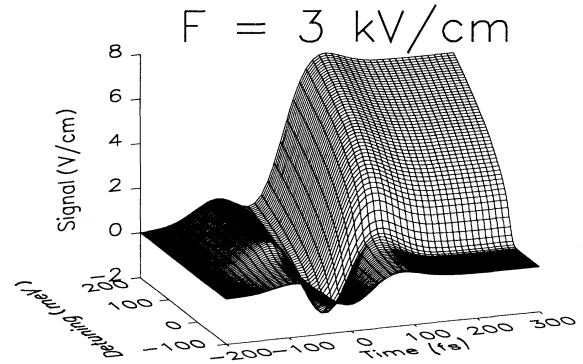


FIG. 11. The radiated signal (85) displays both transport and displacement contributions (cutoff length is $1 \mu\text{m}$).

For the purposes of the numerical calculations below we have set $S=3 \text{ mm}$, $z=1 \mu\text{m}$, $r_0=10 \text{ cm}$, and $\epsilon=12.3$, but since these factors are different for different experimental setups, in fact this choice is intended to just give the right order of magnitude.

Figure 11 displays the terahertz signal (85) for a moderately strong field of 3 kV/cm versus the detuning and time. At negative detunings only the displacement signal caused by the virtual carriers is present, and its temporal wave form follows the second derivative of the excitation intensity in accordance with (80), so that it is negative near the center of the excitation pulse. As the detuning becomes positive, alongside this displacement contribution there also appears a transport contribution:

Figure 13 shows how the temporal wave form evolves with the field. At low fields the displacement signal clearly prevails, then with increasing F the transport signal gradually compensates the negative part of the curve.

Although our theory does not include a number of factors that can affect these predictions *quantitatively*, the

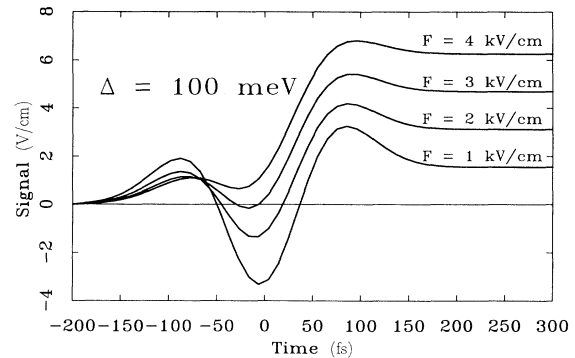


FIG. 13. Field dependence of the temporal wave form of the signal (85). Again the crossover from displacement to transport-dominated behavior is evident. The transport signal does not go to zero at later times because there are no scattering processes in the theory.

above described *qualitative* picture of competition between *transport* and *displacement* currents is quite general and seems to be consistent with the experimentally observed changes in wave forms of the signal with increased detuning.^{1,5}

V. CONCLUSIONS

In this paper, we have considered the ultrafast photoexcitation of carriers in a bulk semiconductor in a dc electric field. Such a field will arise naturally in the surface depletion region, even without an applied external field. We have formulated a density-matrix approach based on an Airy function representation¹⁵ that allows us to incorporate two important features. (1) In a dc electric field, the eigenstates are not characterized by a single \mathbf{k} vector. As a result, unlike the zero-field case, optical transitions are possible between an electron in the valence band and more than one state in the conduction band. (2) For femtosecond pulses, the transition energy is not well defined, and one can no longer use the conventional picture of energy-conserving interband transitions. This formalism allows us to treat both particle current and displacement current and their respective contributions to the radiated field.

The main results of our work can be best formulated in the language of traditional wave-particle dilemma of quantum mechanics: it is impossible to understand the behavior of carries under femtosecond excitation conditions assuming them to be either perfectly localized particles or completely delocalized waves. Instead, one has to treat carriers as localized wave packets formed out of delocalized stationary states (the Airy functions), and the size and shape of these wave packets proves crucial to the determination of observable quantities such as the photocurrent.

Our formalism reproduces the classical motion of the particles in the dc field and also determines the quantum corrections to the classical picture. Using an Airy representation¹⁵ has enabled us to get most of our results analytically. Our results suggest that real carriers (excitation far above the band gap) behave more or less like classical particles and are responsible for transport current, while virtual carriers (excitation far below the band gap) largely determine the displacement part of the current and behave like delocalized “waves.” This different behavior of real and virtual carriers indicates that the conventional viewpoint¹² of virtual carriers having exactly the same properties as the real ones is inapplicable. We also find that there is an intermediate regime (excitation close to the band gap) where both transport and displacement contributions are important, so the above statements about real and virtual carriers are true only asymptotically (at large positive and large negative detunings, respectively).

Within our simple two-band model we are able to calculate only the resonant part of the polarization and had to use a cutoff procedure to get rid of the contributions of virtual carriers in states that are far from the excitation energy. The accurate calculation of these nonresonant contributions requires the knowledge of the full band structure and is beyond the scope of the present work.

The geometrical cutoff that we use here is a simple way to resolve the divergence problem without complicating the model but has the disadvantage of introducing a cutoff parameter that is not very well defined.

Note that our results for the virtual carriers cannot be viewed as a nonlinear optical polarization at zero frequency induced by the optical field and the dc field $P^{(3)} = \chi^{(3)} |E(\omega)|^2 F$ (optical rectification)^{4,6} even though the polarization adiabatically follows the optical field, because the relevant dc fields cannot be treated perturbatively, and in our nonperturbative formalism the polarization is not proportional to the dc field. The real carriers also cannot be described in the language of nonlinear optics because they do not follow the excitation adiabatically (the concept of “dynamic nonlinearities”¹² would be more appropriate here).

In general there can be a nonlinear-optical contribution to the experimentally measured signal that is not included in our theory. Technically, it would stem from the distortion of periodic parts of crystal wave functions by the dc field that was left out here because for typical dc fields it is very small (simple estimates show that the relative contribution to the dipole moment due to this band-structure distortion is of the order of $\mu F/E_g \sim 10^{-4}$). In noncentrosymmetric crystals like GaAs and InP there would also be a nonzero $\chi^{(2)}$ term describing the optical rectification proper: a static dielectric polarization adiabatically following the optical excitation. This term should be independent of the dc field and is highly anisotropic, unlike the electronic contribution that was calculated here. It is much harder to estimate without the detailed knowledge of crystal wave functions, but experiments⁴ suggest that it is important at least in the high-excitation regime where the depletion field should be screened out by the huge number of photocarriers. Indeed, the orientational dependence of the signal observed in some experiments^{4,5} is a characteristic signature of the bulk $\chi^{(2)}$ contribution.

Apart from this nonlinear-optical contribution, there are also a number of other factors that should be included in the theory before it can be quantitatively compared with the experiments. Excitonic effects can be expected to alter the density of states around the band gap and can significantly change the behavior of carriers in this spectral range. The inclusion of scattering processes is also crucial to achieve the correct description of the signal at later times (in our theory the transport signal stays constant after the excitation which is unphysical). Moreover, we do not consider screening of the dc field by the photocarriers, so that our results can be expected to work only in the extreme low-density limit. However, we believe that the free-electron case has to be properly understood before one can start incorporating these phenomena into the theory of transient photocurrent, and the present work constitutes a first step in this direction.

ACKNOWLEDGMENTS

This work was supported by the U.S. Office of Naval Research through Grant No. N00091-JJ-1956. The authors acknowledge useful discussions with S. Obukhov, B. B. Hu, D. Dykaar, P. Saeta, and M. Nuss.

- ¹X.-C. Zhang, B. B. Hu, J. T. Darrow, and D. H. Auston, *Appl. Phys. Lett.* **56**, 1011 (1990); B. B. Hu, X.-C. Zhang, and D. H. Auston, *Phys. Rev. Lett.* **67**, 2709 (1991).
- ²P. C. M. Planken, M. C. Nuss, W. H. Knox, D. A. B. Miller, and K. W. Goossen, *Appl. Phys. Lett.* **61**, 2009 (1992); P. C. M. Planken, M. C. Nuss, I. Brener, K. W. Goossen, M. S. C. Luo, S. L. Chuang, and L. Pfeiffer, *Phys. Rev. Lett.* **69**, 3800 (1992).
- ³N. Katznellenbogen and D. Grischkowsky, *Appl. Phys. Lett.* **58**, 222 (1991).
- ⁴S. L. Chueng, S. Schmitt-Rink, B. I. Greene, P. N. Saeta, and A. F. J. Levi, *Phys. Rev. Lett.* **68**, 102 (1992).
- ⁵X.-C. Zhang, Y. Jin, K. Yang, and L. J. Schowalter, *Phys. Rev. Lett.* **69**, 2303 (1992).
- ⁶Y. Yafet and E. Yablonovich, *Phys. Rev. B* **43**, 12 480 (1991); E. Yablonovich, J. P. Heritage, D. E. Aspnes, and Y. Yafet, *Phys. Rev. Lett.* **63**, 976 (1989).
- ⁷G. M. Wysin, D. L. Smith, and A. Redondo, *Phys. Rev. B* **38**, 12 514 (1988).
- ⁸A. S. Vengurlekaar and S. S. Jha, *Phys. Rev. B* **38**, 2044 (1988).
- ⁹L. Landay and E. M. Lifshitz, *Quantum Mechanics, Nonrelativistic Theory* (Pergamon, London, 1958); J. Callaway, *Quantum Theory of the Solid State* (Academic, New York, 1991), p. 498.
- ¹⁰A. V. Kuznetsov, *Phys. Rev. B* **44**, 8721 (1991).
- ¹¹M. Lindberg and S. W. Koch, *Phys. Rev. B* **38**, 3342 (1988).
- ¹²For a review, see S. Schmitt-Rink, D. S. Chemla, and D. A. B. Miller, *Adv. Phys.* **38**, 89 (1989).
- ¹³G. D. Mahan, *Many-Particle Physics* (Plenum, New York, 1990), p. 199.
- ¹⁴S. Mukamel and H. X. Wang, *Phys. Rev. Lett.* **69**, 65 (1992).
- ¹⁵R. Bertoni and A. P. Jauho, *Phys. Rev. Lett.* **68**, 2826 (1992).